

### Finite-length scaling of collapsing directed walks

T. Prellberg,\* A. L. Owczarek,† R. Brak,‡ and A. J. Guttmann§

Department of Mathematics, The University of Melbourne, Parkville, Victoria 3052, Australia

(Received 8 January 1993)

We study the finite-length scaling of self-interacting partially directed self-avoiding walks utilizing enumeration data up to a total length of 6000 steps. This facilitates the evaluation of the numerical techniques available for calculating exponents at the  $\theta$  (critical) point and in the collapsed phase of walk-type models. Another consequence is the conjecture of an alternative scaling theory for the collapsed region of the phase diagram and the suggestion that this should be applicable to the wider range of undirected problems including interacting self-avoiding walks. We provide a phenomenological picture of the phase transition in terms of the condensation of droplets that allows us to understand the various length scales involved in the problem.

PACS number(s): 05.50.+q, 05.70.Fh, 61.41.+e

#### I. INTRODUCTION

Substantial progress has been made on the elucidation of the properties of an isolated polymer chain [1] from various lattice models in statistical mechanics. Mostly, these have been based upon *self-avoiding walks* (SAW) which have been studied on a variety of lattices and in several dimensions. A canonical example is the interacting SAW (ISAW) model on a regular lattice where attractive nearest-neighbor interactions introduce a thermal field. Two-dimensional systems are often of interest from a directly physical point of view and coupled with the recent enthusiasm [2] for lattice models in two dimensions it comes as no surprise to find a wealth of work on the ISAW on two-dimensional lattices [3]. Many results have been conjectured for this model though no exact solution exists.

A closely related model, that of partially directed walks with similar self-interactions (IPDSAW), has been proposed as a viable alternative to shed some light on the ISAW problem [4]. We have undertaken a thorough study of this model and several results have already been found including much exact information [5,6] (see also the related work on this model with the addition of a boundary [7-9]). The scaling of the properties of walk systems with the length of the walk is the fundamental information required from these models and while much can be inferred from analysis, it is difficult to compute these properties directly. Moreover, it is interesting to compare the finite-length estimates of quantities to the exact values known in the thermodynamic limit. Here, we shall describe a complete study of the scaling of the system with walk length in an attempt to draw some wider conclusions about interacting walk problems. In doing so we shall not only provide a phenomenological picture of the behavior of the model, but also expose generic features of these problems as yet unrecognized. This work has provided the impetus for two recent papers [10,11].

Partially directed walks are self-avoiding walks that have only steps in the positive  $x$  (horizontal) direction

while having steps in both positive and negative vertical directions. In Fig. 1 an allowed configuration is shown, including a representation of which steps (representing monomers) interact. The basic problem is that of evaluating the canonical partition function, given by

$$Q_L(T) = \sum_{\text{configurations}} c_L(I)\omega(T)^I, \tag{1}$$

where  $\omega = \exp(J/k_B T)$ ;  $J$  being some positive coupling constant. Here,  $c_L(I)$  is the number of allowed configurations of length  $L$  that have  $I$  interacting sets of monomers. The thermodynamic limit is given by  $L \rightarrow \infty$  and hence the free energy per monomer is given by

$$f_\infty(T) = -k_B T \lim_{L \rightarrow \infty} \frac{1}{L} \ln Q_L(T). \tag{2}$$

A common procedure is to consider instead the generalized canonical ensemble and introduce a fugacity  $z$  for the walk length. The generalized partition function, or equivalently a generating function, is then found from summing over walk lengths as

$$G(z, \omega(T)) = \sum_{L=0}^{\infty} z^L Q_L(T). \tag{3}$$

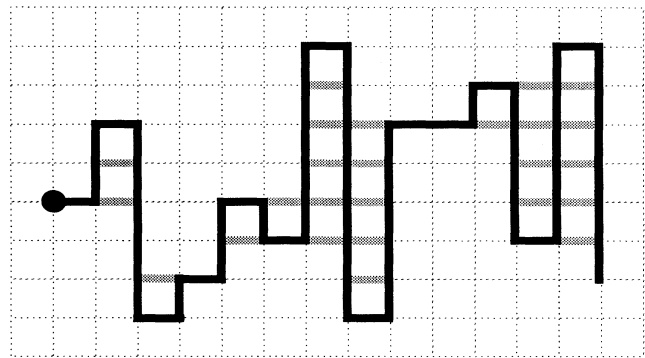


FIG. 1. A typical partially directed walk with interactions represented by grey bonds between nearest-neighbor steps.

It is then not too difficult to show that the closest singularity to the origin,  $z_\infty$  say, of  $G(z, \omega)$  (considering  $z$  the variable and  $\omega$  as a parameter) is related directly to the canonical free energy as

$$z_\infty = \exp[f_\infty(T)/k_B T]. \quad (4)$$

It is, however, not guaranteed *a priori* that all averages of properties in one ensemble will tally with the other [12].

In the analytic work already presented [6] the discussion has centered on the generating function  $G(z, \omega)$  and its derivatives [including extensions to  $G(z, \omega)$ ]. Thermodynamically, the free energy contains a lone singularity, or critical point at some finite temperature. The behavior of the thermodynamic free energy  $f_\infty(T)$ , the internal energy  $u_\infty(T)$ , and the specific heat  $c_\infty(T)$  as functions of temperature are given in Fig. 2. This has been viewed as analogous to a similar behavior in the ISAW problem where the critical point is understood as a collapse transition. Aptly named, this transition signifies the abrupt change of finite-length scaling of the average size of the walks and is believed to be associated with the  $\theta$ -point transition in polymer systems. Hence the study of this transition in the IPDSAW system is of some importance for the understanding of the ISAW model.

As pointed out by Nordholm [12], the relationship between the two ensembles is clear at high temperatures down to and including the critical point in these systems. Therefore, analysis in the generalized ensemble can be confidently translated to the canonical. However, at low temperatures the situation is not well understood. Here the generating function converges at its radius of convergence and quantities such as the average length are finite. It is clear then that taking the limit of going to the radius of convergence is not always the same as the limit  $L \rightarrow \infty$ . This breakdown of the connection between the ensembles provides the stimulus for numerical techniques to be employed. However, knowing how to solve for the generating function allows much more to be achieved by series analysis than for a completely unsolved problem. We, of course, can also confirm that appropriate exponents are the same in both ensembles when required by

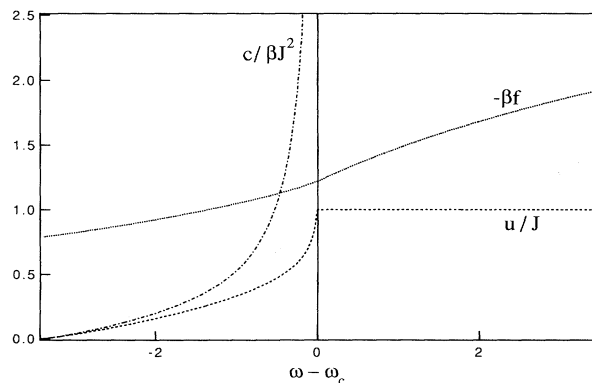


FIG. 2. Plots of the thermodynamic limit free energy  $f_\infty(T)$ , internal energy  $u_\infty(T)$ , and specific heat  $c_\infty(T)$  against the temperature variable  $\omega$  calculated from a continued-fraction expansion [6]. The specific heat is zero for  $\omega > \omega_c$ .

theory. In addition, even for the generating function some effectively numerical work needs to be done to extract some exponents because of the nature of the solution as the functions involved are not well understood [6].

So the first benefits of this study are simply the quantitative understanding of the low-temperature phase of this system and the confirmation that the exact results do hold at higher temperatures. The former of these has led us in two directions.

First, the collapsed phase has not been well understood for any walk problems. As a step towards a better understanding we will consolidate a scaling theory for the partition function for  $T \leq T_c$  introduced by Owczarek, Prellberg, and Brak [10] and subsequently expanded to a full scaling theory of the collapse transition [11]. This scaling theory is partly based on a connection with the droplet model of fluid condensation [13] and can be viewed as a nontrivial example of a model displaying some of the behavior of the fluid model while also having additional features.

The scaling suggested in [10] has been discussed in other contexts such as fluid condensation [13], percolation [14], and models of polymer melts [15–22]. The main idea in each is the addition of a “surface” term in the free energy. However, the dense polymer phase (finite concentration), which is the subject of that last set of papers, sometimes displays the scaling form we have proposed for the collapsed phase (single polymer in an infinite volume) but this form arises from a *different physical reason*. In the dense polymer models the “surface” term is due to the lattice boundary (physically, the container) while we claim that the fractal object that a single polymer forms in the collapsed phase has its own intrinsic polymer surface. We note that the existence of the “surface” term in the dense polymer model is dependent on boundary conditions. We also mention that the dense polymer phase is believed to be related to the low-temperature phase of the *critical*  $O(n)$  model while the collapse phase of isotropic polymers may be related to a phase boundary in the *tricritical*  $O(n)$  model and so are *a priori* unrelated. Hence the scaling form suggested in [10] is indeed an interesting proposal for the *collapsed* polymer phase.

The second benefit of looking more closely numerically at this problem and especially at the collapsed phase is the development of a phenomenological picture of the transition which we have inferred from a detailed study of the length scales involved. These length scales include the end-to-end distances in the two directions (as this is a directed problem). A physical “bubble” or droplet picture can be put forward as a heuristic explanation of the behavior of the length scales. It is commonly assumed that it does not matter what one chooses to measure, the radius of gyration or the end-to-end distance, to find the length scale of global importance. We show how this assumption about length scales can fail at low temperatures, at least in directed problems.

Another reason for undertaking this numerical work is a comparison with other work on the ISAW problem. Again this provides us with an opportunity to give some insight into the procedures employed elsewhere. The

analogous critical point in the ISAW problem has been understood to be a tricritical point in an extended “phase” diagram. This diagram is often taken as either the  $(z, \omega)$  plane or the  $(T, L)$  plane. It has recently been shown that it is reasonable to identify a tricritical-like point in the  $(z, \omega)$  plane or singularity diagram. This diagram for the IPDSAW system is given in Fig. 3. We have verified [6] in the generalized ensemble of the IPDSAW system that the generating function does indeed have the crossover form, and we have calculated the high-temperature exponents and critical exponents. Now with the added understanding of the low-temperature radius of convergence line as a line of condensationlike (first-order) singularities, we are certainly able to see the point as tricritical-like. Moreover, there exist unconfirmed conjectures [3] of the tricritical exponent values in the ISAW problem. In particular, the crossover exponent has been the subject of some dispute. We give a numerical reason why the estimates of that value may be far from their true values. This involves the exponent relation  $2 - \alpha = 1/\phi$ , where  $\alpha$  is the divergence index for the canonical specific heat and  $\phi$  is the crossover exponent. We reveal that while this relationship does indeed hold in the thermodynamic limit it is very slowly asymptotically correct. Corrections to scaling strongly affect numerical estimates. Hence, the use of the relation can lead to erroneous results since it is often assumed to strictly hold in finite-length studies.

The paper is divided into three main sections. The first section presents the model and the method used to generate the enumeration data. The second section explains the results of studying the partition function. The warning concerning the crossover exponent is supported here with numerical evidence. The scaling at low temperatures leads to the Fisher droplet model extension and the walk exponents. In the third section the length scales of the problem are examined and the phenomenological picture of the collapse transition is revealed.

## II. THE METHOD OF ENUMERATION

Here, we describe the model and then present the method of generating the series enumeration data used in our analysis.

The configurations of this model are partially directed walks on a two-dimensional square lattice with nearest-

$$Q_L(x, y, \omega) = \sum_{N=1}^L x^N \sum_{|r_1|+|r_2|+\dots+|r_N|=L-N} y^{L-N} \omega^{u(r_1, r_2, \dots, r_N)}, \quad (7)$$

where we have set  $\omega = \exp(\beta J)$ .

In order to derive an efficient computational scheme for  $Q_L(x, y, \omega)$ , it is convenient to consider the partition functions  $Z_L^{(r)} = Z_L^{(r)}(x, y, \omega)$  for walks of total length  $L+1$  which start with a vertical segment of height  $r$ , then

$$Q_{L+1}(x, y, \omega) = \sum_{r=-L}^L Z_L^{(r)}. \quad (8)$$

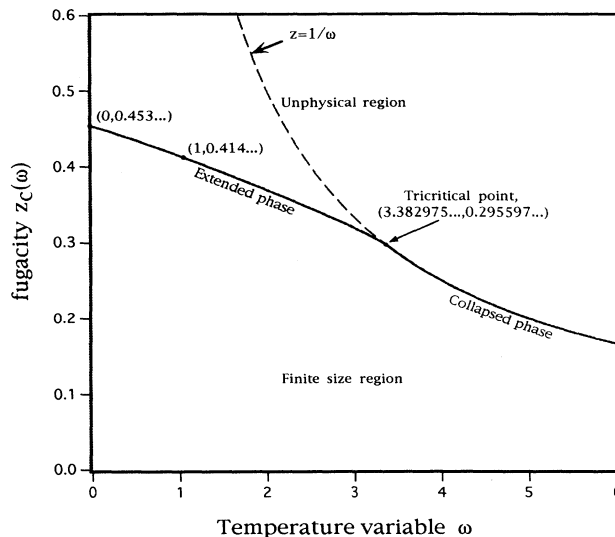


FIG. 3. The singularity diagram for the discrete IPDSAW model. Important points, including free walks at  $\omega=1$  and the tricritical collapse point, are shown.

neighbor interactions. For convenience, we demand that these walks end with a horizontal segment. Due to the directed nature of this problem, we can describe these configurations in a natural way through the distance  $r_i$  between two horizontal steps, measured in the positive  $y$  direction (i.e., the length of the vertical segment is  $|r_i|$ ). Thus, we associate to each configuration an  $N$ -tuple  $(r_1, r_2, \dots, r_N)$  corresponding to a configuration of total length  $L = \sum_{i=1}^N |r_i| + N$ .

The energy due to the nearest-neighbor interactions for each of these configurations is

$$U(r_1, r_2, \dots, r_N) = -Ju(r_1, r_2, \dots, r_N), \quad (5)$$

where

$$u(r_1, r_2, \dots, r_N) = \sum_{i=1}^{N-1} \min(|r_i|, |r_{i+1}|) \mathcal{H}(-r_i r_{i+1}), \quad (6)$$

with  $\mathcal{H}(x)$  being the Heaviside step function. We assign weights  $x$  for steps in the horizontal direction and  $y$  for steps in the vertical direction. The canonical partition function is

(In the definition of  $Z_L^{(r)}$  we have chosen  $L+1$  instead of  $L$ , as it makes the indexing in the following equations more transparent.)

We can concatenate these walks to get a recursion relation for  $Z_L^{(r)}$  as follows:

$$Z_L^{(r)} = xy^{|r|} \left\{ \delta_{r,L} + \sum_{s=-L+r+1}^{L-r-1} \omega^{u(r,s)} Z_{L-r-1}^{(s)} \right\} \quad (9)$$

for  $r = -L, \dots, L$  and  $L = 0, 1, 2, \dots$ . It is this recur-

sion relation which enables us to obtain very long series. Note that

$$Z_L^{(0)} = xQ_L(x, y, \omega). \quad (10)$$

One can further use the symmetry  $Z_L^{(r)} = Z_L^{(-r)}$  and restrict to  $r \geq 0$ , then

$$Z_L^{(r)} = xy^r \left\{ \delta_{r,L} + \sum_{s=0}^{L-r-1} Z_{L-r-1}^{(s)} + \sum_{s=1}^{L-r-1} \omega^{\min(r,s)} Z_{L-r-1}^{(s)} \right\}. \quad (11)$$

Considering  $Z_L^{(r)}$  as a matrix with indices  $L$  and  $r$  shows that we have to recursively compute rows of a triangular matrix.

For the computation of the free energy  $f_L(\omega)$ , internal energy  $u_L(\omega)$ , and specific heat  $c_L(\omega)$ , we need to compute first- and second-order derivatives of  $Z_L^{(r)}$ , further denoted by  $Z_{L,1}^{(r)}$  and  $Z_{L,2}^{(r)}$ . Setting  $x=y=1$  then yields the iteration scheme

$$Z_L^{(r)} = \sum_{s=0}^{L-r-1} Z_{L-r-1}^{(s)} + \sum_{s=1}^{L-r-1} \omega^{\min(r,s)} Z_{L-r-1}^{(s)} + \delta_{r,L}, \quad (12)$$

$$Z_{L,1}^{(r)} = \sum_{s=0}^{L-r-1} Z_{L-r-1,1}^{(s)} + \sum_{s=1}^{L-r-1} \omega^{\min(r,s)} [Z_{L-r-1,1}^{(s)} + \min(r,s) Z_{L-r-1}^{(s)}], \quad (13)$$

$$Z_{L,2}^{(r)} = \sum_{s=0}^{L-r-1} Z_{L-r-1,2}^{(s)} + \sum_{s=1}^{L-r-1} \omega^{\min(r,s)} [Z_{L-r-1,2}^{(s)} + 2 \min(r,s) Z_{L-r-1,1}^{(s)} + \min(r,s)^2 Z_{L-r-1}^{(s)}]. \quad (14)$$

Defining  $a_L(\omega) = (1/L) \ln Z_L^{(0)}$  and recalling  $\omega = \exp(\beta J)$ , we then have

$$f_L(\omega) = -\frac{1}{\beta} a_L(\omega) = -\frac{1}{\beta L} \ln Z_L^{(0)}, \quad (15)$$

$$u_L(\omega) = J \omega \frac{d}{d\omega} a_L(\omega) = \frac{J}{L} \frac{Z_{L,1}^{(0)}}{Z_L^{(0)}}, \quad (16)$$

$$c_L(\omega) = \beta J^2 \left\{ \omega \frac{d}{d\omega} \right\}^2 a_L(\omega) = \frac{\beta J^2}{L} \left\{ \frac{Z_{L,2}^{(0)}}{Z_L^{(0)}} - \left[ \frac{Z_{L,1}^{(0)}}{Z_L^{(0)}} \right]^2 \right\}. \quad (17)$$

In the computation we rescale the matrix coefficients in the iteration scheme because they grow exponentially. As our computations concern the critical point and collapsed phase, this growth is given by  $\omega^{L-r}$ , so that we actually store  $z_L^{(r)} = \omega^{r-L} Z_L^{(r)}$ .

For the computation of the length-scale exponents, we take partial derivatives of (11) with respect to  $x$  and  $y$  and set up a corresponding iteration scheme. For the computation of the vertical end-to-end distance it is further necessary to distinguish between steps in the positive and negative directions; a straightforward but rather tedious generalization of (9) similar to (A1) of [6] is required to accomplish this task.

All the computations have been done using floating-point numbers with 17-digit precision, some up to  $L=6000$ . Therefore it is necessary to discuss the accuracy of these enumerations as opposed to “exact” enumerations with symbolic manipulation programs. One observes that the terms in the sums are positive and decrease exponentially fast in  $\omega$  for  $\omega \geq \omega_c$ . This implies that each of these sums is dominated by only a few terms, and the number of terms contributing to within the floating-point accuracy is in any case less than 50. Therefore roundoff errors are negligible and the scheme is nu-

merically stable within the given floating-point accuracy. A comparison with results from exact enumeration data (computed up to  $L=160$ ) [23] and computations with 34-digit accuracy (computed up to  $L=1000$ ) support this conclusion.

The evaluation of the data involves two different methods. We compute effective exponent estimates, that is, assuming that a quantity grows as

$$f(L) \sim L^\lambda \quad (18)$$

we define an effective exponent as

$$\lambda(L) = \frac{\ln f(L) - \ln f(L-1)}{\ln L - \ln(L-1)} \quad (19)$$

and treat the resulting series with various series extrapolation methods. Note, in this paper we take  $f(x) \sim g(x)$  to mean  $\lim_{x \rightarrow x_0} f/g = \text{const} \neq 0$  (rather than 1). This avoids the frequent introduction of constants. It turns out that we can determine the order of the corrections to scaling quite accurately and can in turn use this information in the extrapolations. This method is then quite successful and gives rather accurate error estimates.

The second method used in the numerical analysis is the method of differential approximants [24,25]. This method confirms our extrapolation results when corrections to scaling are explicitly accounted for. A well-known problem here is also the quite subjective determination of error bounds from the various approximants. However, for shorter series this method gives results closer to the exact values.

### III. RESULTS FOR THE PARTITION FUNCTION

The canonical partition function is expected to have the following length scaling form at high temperatures:

$$Q_L \sim \mu^L L^{\gamma-1}, \quad (20)$$

where  $f_\infty(T) = -k_B T \ln \mu(T)$  and  $\gamma = \gamma_+$  for  $T > T_c$  and  $\gamma = \gamma_t$  for  $T = T_c$ . As previously mentioned the exponent  $\gamma$  can be extracted from the generating function provided the form (20) holds. In this section we will be interested in two topics. First, we will discuss the ease of calculating exponents when the critical-point crossover occurs and, second, we will discuss the form of the finite-length scaling for the partition function at low temperatures where (20) does not hold.

**A. Critical point**

Around the critical point the partition function should have the crossover scaling form [11], which is closely related to a tricritical scaling form (as mentioned in the Introduction),

$$Q_L(\omega) \sim [\mu_a(\omega)]^L L^{\gamma_t - 1} \Theta(\delta\omega L^\phi), \tag{21}$$

where  $\delta\omega = \omega_c - \omega$ ,  $\mu_a(\omega)$  is the analytic part of  $\mu$ , and

$$\Theta(x) \sim \begin{cases} \mu_+^{x^{1/\phi}} x^{(\gamma_+ - \gamma_t)/\phi}, & x \rightarrow \infty \\ 1, & x \rightarrow 0, \end{cases} \tag{22}$$

where  $\mu_+$  is related to the singular part of the free energy.

The canonical specific heat  $C_L(\omega)$  should also have a crossover scaling form

$$c_L(\omega) \sim L^{\alpha\phi} \Omega(\delta\omega L^\phi), \tag{23}$$

where

$$\Omega(x) \sim \begin{cases} x^{-\alpha}, & x \rightarrow \infty \\ 1, & x \rightarrow 0. \end{cases} \tag{24}$$

It has been shown [11] under some general assumptions that the exponent relation

$$2 - \alpha = 1/\phi \tag{25}$$

should hold. Even though there exists an exact solution in the generalized ensemble, we have used series analysis to find estimates of the values of the two exponents  $\alpha$  and  $\phi$  from canonical finite-length data in an attempt to evaluate the numerical precision of the series analysis. As an aside we have verified that the canonical exponent  $\gamma_t$  has indeed the same value as the exact generalized canonical answer.

Our computation of these exponents is greatly aided by the fact that we know the critical temperature and the free energy at the critical point exactly. Therefore, we can compute the exponents from

$$Q_L(\omega_c) \omega_c^{-L} \sim L^{\gamma_t - 1}, \tag{26}$$

$$1 - u_L(\omega_c)/J \sim L^{-(1-\alpha)\phi}, \tag{27}$$

$$c_L(\omega_c) \sim L^{\alpha\phi}. \tag{28}$$

In Figs. 4 and 5 we plot the effective exponents for  $\alpha$ ,  $\phi$ , and  $\alpha + 1/\phi$ . One can immediately see that the “true” values of these quantities, being  $\frac{1}{2}$ ,  $\frac{2}{3}$ , and 2, are only slowly reached. This presents a warning in the wider field of walk problems at a collapse transition when extra-

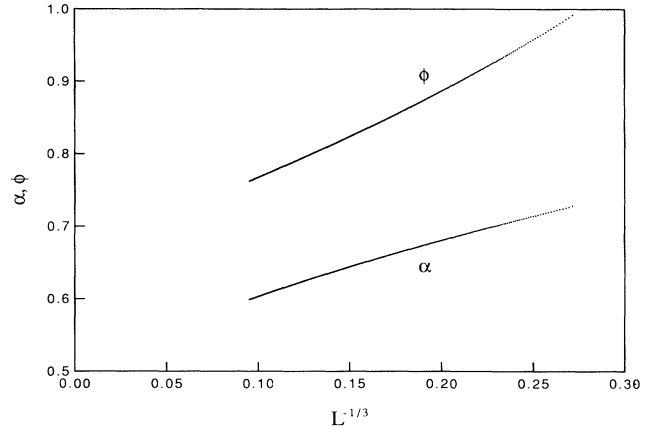


FIG. 4. Estimates for the exponents  $\alpha$  and  $\phi$  at the collapse transition are plotted against a corrections-to-scaling term of  $L^{-1/3}$  for  $L$  up to 2000. The exact values are  $\frac{1}{2}$  and  $\frac{2}{3}$ , respectively. This plot shows that the series are only slowly convergent.

polating finite-length data, a topic which has been discussed in some detail elsewhere [11].

We further analyze these data using two techniques. First, from the figures we see that the correction terms are of order  $L^{-1/3}$ , therefore we also extrapolate towards  $L = \infty$  by fitting to an expansion in powers of  $L^{-1/3}$  and get good results. Second, second- and third-order inhomogeneous differential approximants are used, with the critical point biased at 1, and we also checked for confluent exponents. We utilized 100 terms each, so that for the 2000-term series only every 20th term was used. The range of the approximants was [23–25, 23–25, 23–25; 20–25] for the second-order approximants and [19–20, 19–20, 19–20, 19–20; 13–17] for the third-order ones. We summarize the results in Table I.

Clearly the extrapolation of the exponents from the 2000-term series with an assumed correction term is most successful. We point out that a similar analysis for the 100-term series does not yield any meaningful results,

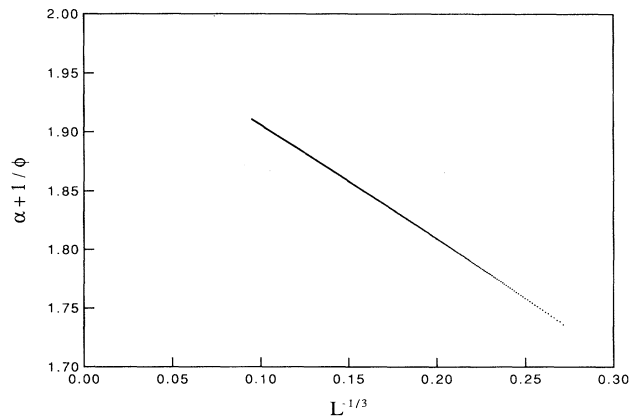


FIG. 5. To demonstrate the slow asymptotic truth of the relation  $2 - \alpha = 1/\phi$  a plot of  $\alpha + 1/\phi$  is shown. The leftmost point corresponds to  $L = 2000$ .

TABLE I. Numerical estimations for  $\gamma_t$ ,  $\alpha$ , and  $\phi$ . The differential approximant estimates shown for  $\alpha\phi$  and  $(\alpha-1)\phi$  correspond to two techniques: In the first row are the results from a simple differential approximant analysis, while the second and third row show the exponent and confluent exponent, respectively (from a confluent singularity analysis). The values shown for  $\alpha$  and  $\phi$  are derived from the simple differential approximant analysis for the short series and from the confluent singularity analysis for the long series.

	Differential approximants				Extrapolation $L \leq 2000$	Exact results
	$L \leq 100$		$L \leq 2000$			
	2nd order	3rd order	2nd order	3rd order		
$\gamma_t$	0.3354(2)	0.3356(1)	0.333 48(1)	0.333 48(1)	0.3333(1)	1/3
$\alpha\phi$	0.47(2)	0.43(2)	0.374(1)	0.377(3)	0.3333(1)	1/3
	0.42(6)	0.41(6)	0.33(3)	0.329(1)		
	not detectable		0.08(3)	0.06(1)		
$(\alpha-1)\phi$	-0.302(1)	-0.304(1)	-0.33(2)	-0.3242(2)	-0.3333(1)	-1/3
	-0.31(3)	-0.31(1)	-0.333(2)	-0.3333(2)		
	not detectable		-0.61(5)	-0.66(1)		
$\alpha$	0.61(3)	0.59(3)	0.50(5)	0.497(2)	0.5000(1)	1/2
$\phi$	0.77(2)	0.73(2)	0.66(3)	0.662(1)	0.6667(1)	2/3
$\alpha+1/\phi$	1.91(5)	1.96(5)	2.0(1)	2.008(3)	2.0000(2)	2

even if the right correction term is assumed. This ties in with the differential approximant analysis which does not indicate any confluent exponent.

If we only had the short series,  $\gamma_t$  would thus have been the only correctly estimated exponent. Strong corrections to scaling make the estimations of  $\alpha$  and  $\phi$  quite problematic and even the “correct” guess of the leading correction term does not improve this. We add that in general such a guess from shorter series is highly dangerous and can even result in a “self-fulfilling prophecy.”

The most important feature in this table is perhaps that the differential approximant method, even if applied to a rather “long” series of 100 terms when compared to its usual applications, gives *wrong* results in the sense that even within quite a conservative error estimation the true value is outside that range. A good check for this is here relation (25), which is *not* satisfied by these 100-term extrapolated exponent values.

Applied to the 2000-term series, on the other hand, the differential approximant method gives a good indication of the existence of the confluent exponent and also gives exponent estimates consistent with (25). However, when compared to the direct extrapolation, one sees that the error is still rather large.

Only with a direct extrapolation with an *a priori* guess of the right correction terms (which by virtue of the consistent result suggests it is itself correct *a posteriori*) can the exponent values be extrapolated to a satisfactory accuracy. As these values satisfy the relation (25) and the differential approximant analysis gives consistent results, this analysis can be trusted.

In summary, we caution again that one can really only have confidence in asymptotic analysis when several methods agree, especially if one does not have any specific information about the form that one is fitting to. Otherwise one is too easily tempted to believe in possibly misleading error bounds.

Furthermore, if we did not know the exact location of

the critical point along with the free energy and internal energy, we would have to resort to the usual procedure of determining the exponents from the scaling of the peak of the specific heat. The results [23] using 100-term series are  $\alpha=1.30(5)$  and  $\phi=0.45(3)$ , with rather subjective error bounds. Since the exact values are  $\frac{1}{2}$  and  $\frac{2}{3}$ , respectively, clearly this method is unsatisfactory. The problems with this last approach are probably due to the strong asymmetry of the collapse transition.

We have calculated the scaling functions  $\Theta(x)$  and  $\Omega(x)$  (see Figs. 6 and 7). These support the crossover scaling theory in the canonical ensemble. One can see also both the asymmetry of the scaling function and the size of the region of validity of the scaling function from these diagrams. The high-temperature side converges very slowly and this reinforces the remarks above and elsewhere [11] concerning the care that must be taken in analyzing finite-length data at collapse transitions.

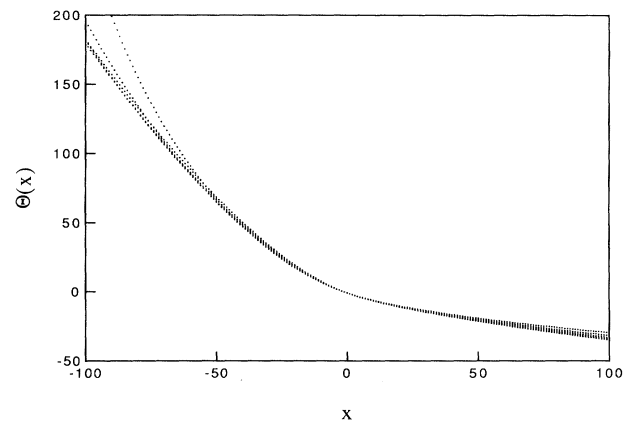


FIG. 6. Estimates for the scaling function  $\Theta(x)$  of the partition function (up to a constant) are shown for lengths  $L=250, 500, 1000, 2000, 4000$ .

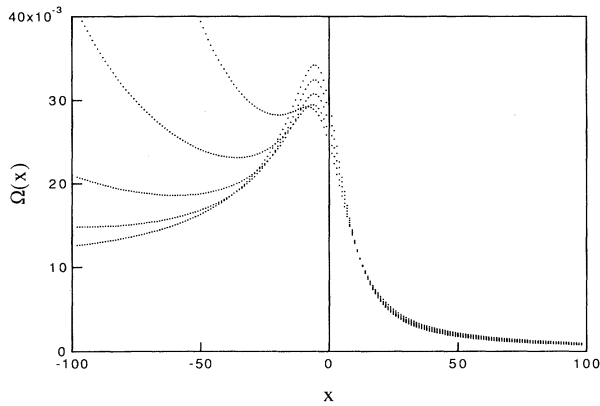


FIG. 7. Estimates for the scaling function  $\Omega(x)$  of the specific heat (up to a constant) are shown for lengths  $L=250, 500, 1000, 2000, 4000$ .

### B. Collapsed phase

The scaling form (20) is the expected scaling form for the partition function in a wide range of walk or polygon models and hence polymer systems. This form induces a divergence in the generating function (see above) as one approaches the radius of convergence from below. From the exact solution [5,6] it is clear that the generating function *converges* at its radius of convergence indicating an essential singularity of some type.

Previous work by Fisher [13] on the condensation of a fluid system can be adapted to this problem in the following way. We have conjectured that the scaling form

$$Q_L \sim [\mu_0(\omega)]^L [\mu_1(\omega)]^{L^\sigma} L^{\gamma_- - 1}, \quad (29)$$

where  $\sigma \approx \frac{1}{2}$ , is the appropriate asymptotic scaling in the collapsed region for general SAW-type problems [10]. We have learned that recent work by Grassberger and Hegger strongly supports our claim for three-dimensional isotropic polymers [26]. Here we shall present evidence to support this claim. We shall also consider the consequences for the critical-point crossover scaling. This will introduce a further critical exponent  $\chi$ , thereby extending Fisher's discussion.

From the exact solution [5,6] we know already that  $\mu_0(\omega) = \omega$ . For the estimation of  $\sigma$ , we first compute an effective exponent  $\sigma(L)$  from

$$\ln[Q_L(\omega)\omega^{-L}] \sim L^\sigma \quad (30)$$

at  $\omega - \omega_c = 1, 2, \dots, 64$  for  $L \leq 6000$  in the collapsed phase. A plot against  $L^{-1/2}$  (Fig. 8) suggests that in fact asymptotically  $\sigma = \frac{1}{2}$  in the collapsed regime. Using differential approximants on  $\ln[Q_L(\omega)\omega^{-L}]$ , we confirm this by the estimate  $\sigma = 0.495(6)$ .

Assuming  $\sigma = \frac{1}{2}$ , we now proceed with an estimation of  $\gamma_- - 1$ . We compute estimates from a two-parameter fit to

$$\ln[Q_L(\omega)\omega^{-L}] \sim \ln\mu_1 L^{1/2} + (\gamma_- - 1)\ln L. \quad (31)$$

The result is shown in Fig. 9 and again we see conver-

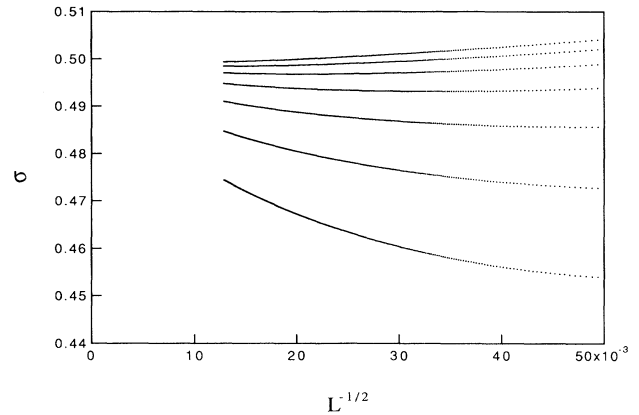


FIG. 8. Estimates for the exponent  $\sigma$  plotted against a corrections-to-scaling term, for a range of temperatures, for  $L$  up to 6000. The "temperatures" are, from top to bottom,  $\omega = \omega_c + 64.0, 32.0, 16.0, 8.0, 4.0, 2.0, 1.0$ .

gence to a value of about 0.75 over a wide range of temperatures in the collapsed region. We remark that due to pathological behavior of the zero-temperature state, these computations need to be done with series whose lengths are well above 100 in order to overcome this pathological behavior.

Extrapolation of estimates of  $\gamma_-$  by fitting successively to

$$\ln[Q_L(\omega)\omega^{-L}] \sim \ln\mu_1 L^{1/2} + (\gamma_- - 1)\ln L + \sum_{i=0}^n a_n L^{-n/2} \quad (32)$$

results in a very accurate determination of  $\mu_1(\omega)$  and a value of  $\gamma_- = 0.250000(5)$ , which by its accuracy is an indirect confirmation of  $\sigma = \frac{1}{2}$ . The direct estimation of  $\sigma$  is less accurate because the differential approximants cannot account for either  $\mu^{L^\sigma}$  asymptotic behavior or,

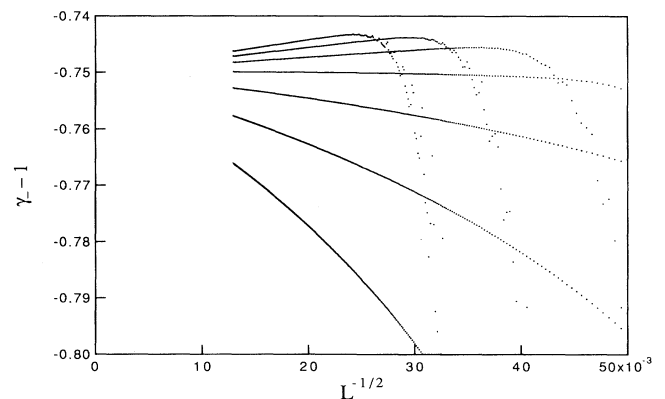


FIG. 9. Estimates for the exponent  $\gamma_- - 1$ , computed by fitting the calculated partition function to the full form (29) for  $L$  up to 6000. Again these cover the same range of temperatures as in Fig. 8 from top to bottom (on the left-hand side). Fitting these curves with third- and fourth-order polynomials in  $L^{-1/2}$  produces remarkably stable results.

upon taking the logarithm, for the  $(\ln L)$ -correction term.

Of further interest is the crossover that occurs as  $\omega \rightarrow \omega_c$ . A crossover scaling form for the collapsed region is again given by

$$Q_L(\omega) \sim [\mu_a(\omega)]^L L^{\gamma_i - 1} \Theta(\delta\Omega L^\phi) \quad (33)$$

(where now  $\delta\omega = \omega_c - \omega < 0$ ) and comparison with (29) implies that

$$\Theta(x) \sim \begin{cases} \mu_-^{|x|^{1/\phi}} \mu_s^{|x|^{\sigma/\phi}} |x|^{(\gamma_- - \gamma_i)/\phi}, & x \rightarrow -\infty \\ 1, & x \rightarrow 0 \end{cases} \quad (34)$$

This, together with (21), describes the complete crossover scaling form as outlined in [11]. [In our model, we have an even slightly simpler scaling form due to  $\mu_a(\omega) = \omega$  and  $\mu_- = 1$  in the collapsed phase.]

To test this scaling form, we note that as a consequence we have asymptotically

$$\mu_1(\omega) \sim \mu_s^{|\delta\omega|^\chi}, \quad \text{with } \chi = \frac{\sigma}{\phi} = \frac{3}{4}, \quad (35)$$

so that the independent computation of the exponent  $\chi$  can serve as a verification. In order to check its predicted value, we compute  $\mu_1(\omega)$  for  $\omega \rightarrow \omega_c$ . We fit again using (31), but now with  $\gamma_-$  specified. Naturally this extrapolation gets worse when we approach  $\omega_c$ , as we have to extrapolate into the crossover regime itself. The results are shown in Fig. 10, and one can see that the error increases as the critical point is approached. Clearly the numerical results are compatible with a slope of  $\chi = \frac{3}{4}$ .

We conclude this section with a summary of the exponent values in the collapsed phase:

$$\sigma = \frac{1}{2}, \quad \gamma_- = \frac{1}{4}, \quad \chi = \frac{3}{4}. \quad (36)$$

#### IV. RESULTS FOR THE LENGTH SCALES

The examination of the ‘‘size’’ of the objects is a central task of the analysis of walk models. We present results on the end-to-end displacements of the walks as

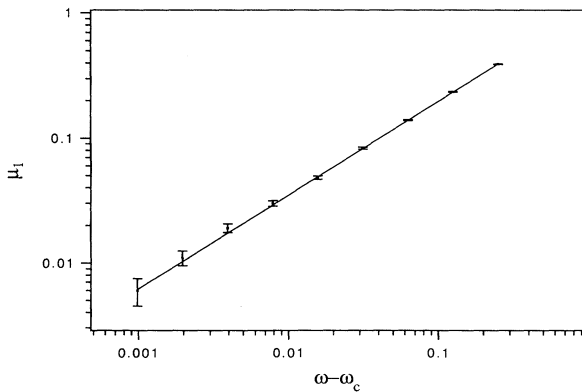


FIG. 10. To provide an estimate for the exponent  $\chi$ , a log-log plot of  $\mu_1$  is given against the ‘‘temperature’’ difference to the critical point  $(\omega - \omega_c)$ . A 6000-term series was used to calculate  $\mu_1$ . The straight line has slope  $\frac{3}{4}$ .

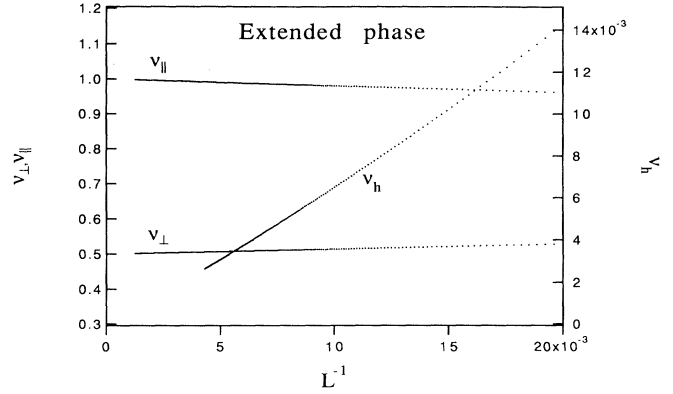


FIG. 11. The high-temperature ( $\omega = 1.0$ ) length-scale exponents can be estimated from this plot of  $v_{\parallel}$ ,  $v_{\perp}$ , and  $v_h$ . The corrections should be of order  $L^{-1}$  (from the exact solution) and so we use this as the variable against which we plot. A 600-term series was used here because of the greater complexity of the series needed to calculate length-scale exponents.

functions of length and temperature and in the following subsection provide a simple phenomenological picture and scaling theory to explain the results.

The quantities of initial interest are the average horizontal  $\langle R_x \rangle$  and vertical  $\langle R_y \rangle$  end-to-end displacements:

$$\langle R_{x,y} \rangle = \sum_{\text{configurations}} R_{x,y} c_L(I) \omega^I / Q_L. \quad (37)$$

These provide some measure of the global size of the walks. Note that, for any walk,  $R_x$  is simply equal to the number of horizontal steps  $L_x$  while this correspondence does not hold for  $R_y$ . One can compute the corresponding generalized canonical averages by introducing three fugacities into the generating function associated with the horizontal steps and with the vertical steps from folds that move in the positive and negative (a different fugacity)  $y$  directions (as one moves along the walk in the posi-

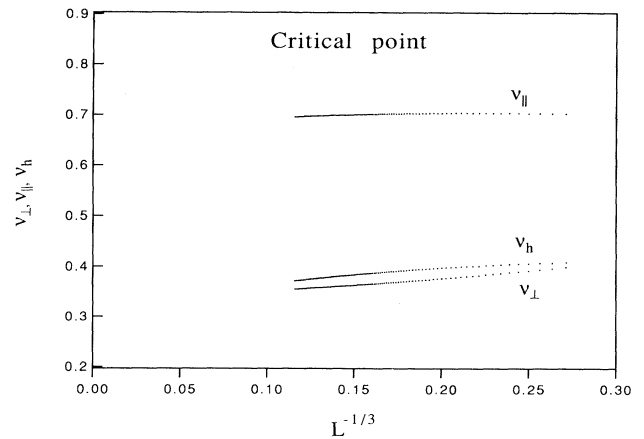


FIG. 12. The critical-temperature ( $\omega = 3.382975 \dots$ ) length-scale exponents can be estimated from this plot of  $v_{\parallel}$ ,  $v_{\perp}$ , and  $v_h$ . Here the corrections to scaling should be of order  $L^{-1/3}$ . A 600-term series was used.



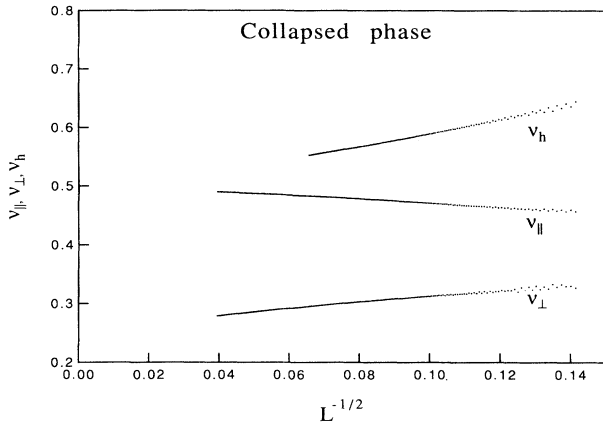


FIG. 13. The low-temperature ( $\omega=6.0$ ) length-scale exponents can be estimated from this plot of  $v_{\parallel}$ ,  $v_{\perp}$ , and  $v_h$ . Here the corrections to scaling should be of order  $L^{-1/2}$ . A 600-term series was used.

tive  $x$  direction) [6]. However, as previously stressed, the low-temperature results are not useful since the generalized canonical averages converge at the radius of convergence of the generating function.

Also of interest is the average length of each vertical fold. This will give a measure of the local size and is defined as

$$\langle h \rangle = \sum_{\text{configurations}} \left[ \sum_i h_i / L_x \right] c_L(I) \omega^I / Q_L, \quad (38)$$

where  $i$  labels the folds of an individual walk and  $h_i = |r_i|$ .

As  $L \rightarrow \infty$  the size of the walks becomes large and the end-to-end displacements are expected to scale as

$$\langle R_{x,y} \rangle \sim L^{v_{x,y}}. \quad (39)$$

We define also  $v_h$  by

$$\langle h \rangle \sim L^{v_h}. \quad (40)$$

Utilizing the recurrence relations, we have calculated effective exponents for  $\langle R_{x,y} \rangle$  and  $\langle h \rangle$  as functions of  $L$  from series up to  $L=600$ . The reason for these much shorter series is that the amount of computer memory needed to keep track of the geometric information is naturally much larger than for the computation of the generating function alone. The results are shown in Figs. 11, 12, and 13.

As above, estimates of the exponents at high, critical, and low temperatures, are shown in Table II. The estimation of the numerical values again used differential

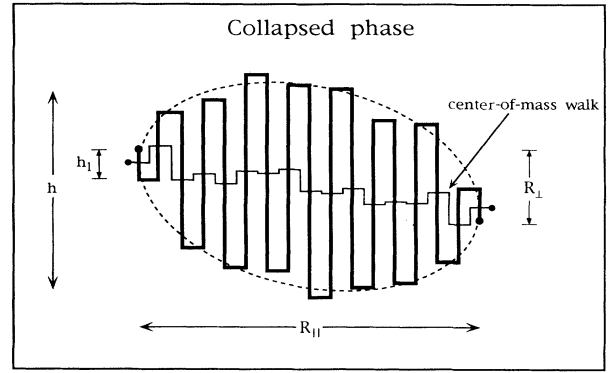


FIG. 14. A picture showing the dominant type of configurations at low temperature; these being described as bubblelike.

approximants as well as an extrapolation procedure with an assumed correction-to-scaling form. The assumed corrections to scaling were integer powers of  $L^{-1}$  in the extended phase,  $L^{-1/3}$  at the critical point, and  $L^{-1/2}$  in the collapsed phase. The high- and critical-temperature exponents agree, as expected, with the exact calculation [6] and have been confirmed by clever scaling arguments [27].

The results for  $T > T_c$  converge quite fast to the exact results of  $v_x=1$ ,  $v_y=1/2$ , and  $v_h=0$ , with the anticipated correction to scaling of  $L^{-1}$ . This allows us to visualize the dominant walk configurations in the extended phase as elongated. They are effectively free partially directed random walks with a finite local fold length. For a later comparison we mention that here the square of the vertical radius of gyration scales in the same way as the square of the vertical end-to-end distance.

At  $T_c$  the estimates converge at a greatly reduced rate to the exact values of  $v_x=2/3$ ,  $v_y=1/3$ , and  $v_h=1/3$ , while the theoretical correction term  $L^{-1/3}$  has a much stronger effect. The predominant walks are now those in which the local length is as large as the overall size. So the radius of gyration, the end-to-end distance and the local size all scale together.

Most curious, at first, are the low-temperature results which are precisely the ones that have not been found exactly. Conventional wisdom would suggest that the walks collapse to compact objects and so any radius of gyration would scale as the length to the exponent  $1/d$ , where  $d$  is the lattice dimension. This view also dictates that it does not matter which length scale one chooses to measure (the actual radius of gyration or the end-to-end distance) as the same exponent should appear. We have

TABLE II. End-to-end displacement and average fold length exponents.

Temperature	$v_x$		$v_y$		$v_h$	
	numerical	exact	numerical	exact	numerical	exact
$T > T_c$	1.00000(1)	1	0.50000(1)	1/2	0.00000(1)	0
$T_c$	0.6668(2)	2/3	0.3338(5)	1/3	0.334(2)	1/3
$T < T_c$	0.501(1)		0.251(1)		0.502(2)	

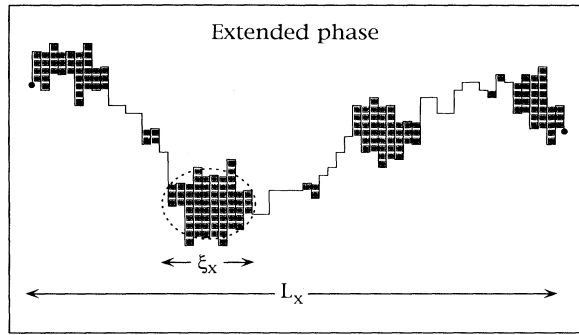


FIG. 15. A picture showing the dominant type of configurations at high temperatures for comparison. Finite-size droplets form up to the size of the thermal correlation length  $\xi_x$ .

found strong evidence that the vertical end-to-end displacement exponent is in fact not  $\frac{1}{2}$  but  $\frac{1}{4}$ . However, with some simple arguments one can show that the global size of the object in the vertical direction must scale with an exponent of at least  $\frac{1}{2}$ . The average local size (that is, the fold length) certainly seems to scale with the exponent  $\frac{1}{2}$ , and the global size must be as large as the local one. In the next section we explain these intriguing results.

#### Scaling theory

The key to understanding these results is to understand that the dominant configurations at low temperatures are droplet or bubblelike. In fact one can view the collapse transition as a fluid condensation transition by placing “particles” on the dual lattice wherever there exist monomer-monomer interactions. Then at high temperatures we have an infinite string of finite droplets (see Fig. 15) while at low temperatures a single infinite drop exists (see Fig. 14).

As the results stand, one feature that is immediately clear is that the relationship

$$v_x = 2v_y \quad (41)$$

always holds. This leads us to the idea that the center of mass of the configurations at any temperature acts like a free partially directed walk. The other ingredient needed to make sense of the  $\frac{1}{4}$  value for  $v_y$  is the following. Let  $h_i$  be the height of the  $i$ th fold in a configuration and  $\langle h_i \rangle$  be the average height over walks of length  $L$ . If we let  $i$  and  $L_x - i$  simultaneously be proportional to  $L_x$  then we can safely assume that  $\langle h_i \rangle \sim L^{1/2}$ . However, if  $v_y = \frac{1}{4}$  then we should have  $v_1 \leq \frac{1}{4}$  where  $\langle h_{L_x} \rangle = \langle h_1 \rangle \sim L^{v_1}$ . We have estimated the value of  $v_1$  (Fig. 16) and found that it is in fact close to zero. We con-

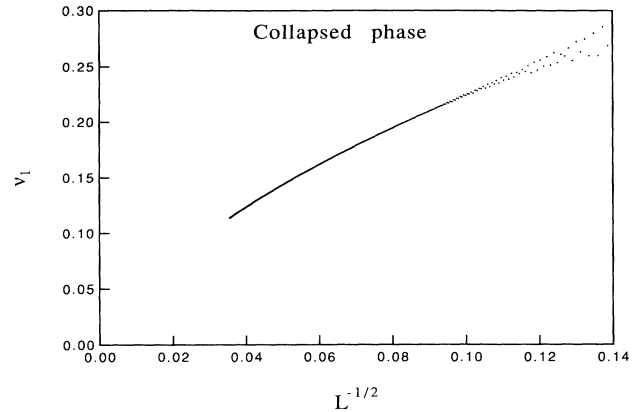


FIG. 16. The growth exponent for the length of the first segment  $h_1$  denoted by  $v_1$  is plotted here against  $L^{-1/2}$ . It clearly converges to a value less than  $\frac{1}{4}$  and probably converges to zero.

ture that it is in fact zero (although we do not comment on whether  $\langle h_1 \rangle$  is finite in the thermodynamic limit). We then see that the dominant configurations are bubblelike, rather than, say, square as one might also expect.

We may introduce a shape scaling form for the bubble as

$$\langle h_i \rangle \sim L^{v_h} H(iL^{-v_x}), \quad (42)$$

where

$$H(x) \sim x^{(v_h - v_1)/v_x} \quad (43)$$

for  $x \rightarrow 0$ . The exponent  $\rho = (v_h - v_1)/v_x$  is a shape exponent describing the shape of the ends of the bubble. In this case  $v_1 = 0$  so  $\rho = 1$  giving a locally linear shape.

To summarize, since the number of “center-of-mass” steps, which is of the order of  $L^{1/2}$ , perform a partially directed walk this “center-of-mass” walk has an average vertical displacement of the order of  $L^{1/4}$ . Given that the length of the first and last segments scale with powers less than  $\frac{1}{4}$ , then the total vertical end-to-end displacement scales as  $L^{1/4}$ . Hence this does not contradict the fact that the global vertical size of the walks scales with the power  $\frac{1}{2}$ , as the walks form bubble-shaped objects on average.

#### ACKNOWLEDGMENTS

The authors thank Keith Briggs for carefully reading the manuscript and are grateful to the Australian Research Council for financial support. They also thank Keith Briggs for his willingness to continually extend his differential approximant program [28] to suit our growing needs.

\*Electronic address: prel@mundoe.maths.mu.oz.au

†Electronic address: aleks@mundoe.maths.mu.oz.au

‡Electronic address: brak@mundoe.maths.mu.oz.au

§Electronic address: tonyg@mundoe.maths.mu.oz.au

[1] J. des Cloizeaux and G. Jannink, *Polymers in Solution*

(Clarendon, Oxford, 1990).

[2] R. J. Baxter, *Exactly Solved Models in Statistical Mechanics* (Academic, London, 1982).

[3] B. Duplantier and H. Saleur, *Phys. Rev. Lett.* **59**, 539 (1987).

- [4] A. R. Veal, J. M. Yeomans, and G. Jug, *J. Phys. A* **23**, L109 (1990).
- [5] R. Brak, A. Guttmann, and S. Whittington, *J. Phys. A* **25**, 2437 (1992).
- [6] A. L. Owczarek, T. Prellberg, and R. Brak, *J. Stat. Phys.* (to be published).
- [7] D. P. Foster, *J. Phys. A* **23**, L1135 (1990).
- [8] D. P. Foster and J. M. Yeomans, *Physica (Utrecht)* **23**, L1135 (1990).
- [9] D. P. Foster, *J. Stat. Phys.* **70**, 1029 (1993).
- [10] A. L. Owczarek, T. Prellberg, and R. Brak, *Phys. Rev. Lett.* **70**, 951 (1993).
- [11] R. Brak, A. L. Owczarek, and T. Prellberg, *J. Phys. A* (to be published).
- [12] K. Sture Nordholm, *J. Stat. Phys.* **9**, 235 (1973).
- [13] M. E. Fisher, *Physics* **3**, 255 (1967).
- [14] D. Stauffer, *An Introduction to Percolation Theory* (Taylor and Francis, London, 1985).
- [15] B. Duplantier and H. Saleur, *Nucl. Phys. B* **290**, 291 (1987).
- [16] B. Duplantier and F. David, *J. Stat. Phys.* **51**, 327 (1988).
- [17] A. Malakis, *Physica (Utrecht)* **84**, 256 (1976).
- [18] G. F. Tuthill and M. V. Jaric, *Phys. Rev. B* **31**, 2981 (1985).
- [19] G. F. Tuthill and Z. Sui, *J. Chem. Phys.* **88**, 8000 (1988).
- [20] G. F. Tuthill, *J. Chem. Phys.* **90**, 5869 (1989).
- [21] G. F. Tuthill, *J. Chem. Phys.* **92**, 3179 (1990).
- [22] G. F. Tuthill and D. J. Glover, *J. Chem. Phys.* **94**, 8408 (1991).
- [23] T. Prellberg and A. J. Guttmann (unpublished).
- [24] A. J. Guttmann and G. S. Joyce, *J. Phys. A* **5**, L81 (1972).
- [25] A. J. Guttmann, in *Phase Transitions and Critical Phenomena*, edited by C. Domb and J. L. Lebowitz (Academic, New York, 1989), Vol. 13.
- [26] P. Grassberger and R. Hegger (unpublished).
- [27] D. Foster, *Phys. Rev. E* **47**, 1411 (1993).
- [28] K. Briggs (private communication).